



Review

Investigation of Surface Layers on Biological and Synthetic Hydroxyapatites Based on Bone Mineralization Process

Kazuto Sugimoto ¹, Yanni Zhou ², Tania Guadalupe Peñaflo Galindo ³, Reo Kimura ² and Motohiro Tagaya ^{2,*}

¹ Department of Materials Science and Technology, Nagaoka University of Technology, Kamitomioka 1603-1, Nagaoka, Niigata 940-2188, Japan

² Department of Materials Science and Bioengineering, Nagaoka University of Technology, Kamitomioka 1603-1, Nagaoka, Niigata 940-2188, Japan

³ General Department, National Institute of Technology, Nagaoka College, 888 Nishikatagai, Nagaoka, Niigata 940-8532, Japan

* Correspondence: tagaya@mst.nagaokaut.ac.jp; Tel.: +81-258-47-9345

Abstract: In this review, the current status of the influence of added ions (i.e., SiO_4^{4-} , CO_3^{2-} , etc.) and surface states (i.e., hydrated and non-apatite layers) on the biocompatibility nature of hydroxyapatite (HA, $\text{Ca}_{10}(\text{PO}_4)_6(\text{OH})_2$) is discussed. It is well known that HA is a type of calcium phosphate with high biocompatibility that is present in biological hard tissues such as bones and enamel. This biomedical material has been extensively studied due to its osteogenic properties. The chemical composition and crystalline structure of HA change depending on the synthetic method and the addition of other ions, thereby affecting the surface properties related to biocompatibility. This review illustrates the structural and surface properties of HA substituted with ions such as silicate, carbonate, and other elemental ions. The importance of the surface characteristics of HA and its components, the hydration layers, and the non-apatite layers for the effective control of biomedical function, as well as their relationship at the interface to improve biocompatibility, has been highlighted. Since the interfacial properties will affect protein adsorption and cell adhesion, the analysis of their properties may provide ideas for effective bone formation and regeneration mechanisms.

Keywords: hydroxyapatite; non-apatitic layer; hydration layer; surface properties; biocompatibility; bone tissue formation; mineralization



Citation: Sugimoto, K.; Zhou, Y.; Galindo, T.G.P.; Kimura, R.; Tagaya, M. Investigation of Surface Layers on Biological and Synthetic Hydroxyapatites Based on Bone Mineralization Process. *Biomimetics* **2023**, *8*, 184. <https://doi.org/10.3390/biomimetics8020184>

Academic Editors: Hamid Nurrohmah and Jinhui Tao

Received: 20 March 2023

Revised: 21 April 2023

Accepted: 25 April 2023

Published: 28 April 2023



Copyright: © 2023 by the authors. Licensee MDPI, Basel, Switzerland. This article is an open access article distributed under the terms and conditions of the Creative Commons Attribution (CC BY) license (<https://creativecommons.org/licenses/by/4.0/>).

1. Introduction

Bone grafting is one of the surgical treatments for bone defects caused by osteoporosis, bone tumors, and bone atrophy in dental implants, and is generally performed by using autologous or allogeneic bone grafts, in which the bone is taken from the patient's own or a compatible donor, and then transplanted into the defect site. However, it presents some problems, such as increased burden on patients due to surgery and limitation of the amount of bone used [1–4]. Synthetic bone has recently been produced as an alternative to autogenous bone to address these problems. Calcium phosphate (CP), hydroxyapatite (HA), ceramics, CP cements, and bioactive glass are generally known as synthetic bone materials [5–7]. Synthetic bone has the advantages of high biocompatibility, fewer and minimal requirements for surgery, and low risk of inflammation; however, it is unable to induce cells associated with bone metabolism from the surrounding tissue after replacing a bone defect. Accordingly, the improvement of the ability to form new bone has been researched. Therefore, it is important to elucidate the mechanism of biological bone formation and to create synthetic bone that resembles biological bone.

Biological bone is composed of an organic matrix, reinforced by the deposition of inorganic salts consisting mainly of Ca^{2+} and PO_4^{3-} , with 30 wt.% of organic matrix and 70 wt.% of inorganic salts. Biological bone is metabolically active, with “bone resorption”, the destruction of old bone, and “bone formation”, the creation of new bone. This cycle of

bone metabolism is physiologically important, and its functions are to replace brittle old bone and to strengthen areas subjected to load [8,9]. Figure 1 shows the bone formation process. Osteocytes are derived from osteoblasts and are formed by the incorporation of osteoblasts into the bone matrix [10]. Osteocytes act as mechanosensory cells because they build networks by joining small tubules together [11]. Due to their function, they are thought to be the cells that detect the mechanical loading of bone and are involved in the activity and generation of osteoblasts and osteoclasts [12]. Bone resorption is carried out by phagocytic multinucleated cells called osteoclasts. These cells originate from monocytes or monocyte-like cells produced in the bone marrow [13]. Bone resorption occurs when osteoclasts come into contact with bone. During this process, proteolytic enzymes released from osteoclast lysosomes dissolve the organic substrate of bone. This mechanism releases several acids, including citric and lactic acids, from mitochondria and secretory vesicles. This phenomenon results in the dissolution of bone composed of Ca^{2+} and PO_4^{3-} [14]. On the other hand, osteoblasts are responsible for bone formation. The mechanism of bone formation begins with the secretion of collagen molecules and substrate substances by osteoblasts. Subsequently, osteoblasts form collagen fibers from the collagen molecules to form allogeneic bone, which incorporates some of the osteoblasts to become osteocytes [15]. Within a few days of the formation of the analogous bone, amorphous calcium phosphate (ACP) begins to precipitate on the surface of the collagen fibers. The precipitated ACP is converted to HA over a period of weeks to months, during which atoms are added or replaced [16,17]. A few percent of HA remains amorphous and is more rapidly absorbed when Ca^{2+} is needed in the extracellular fluid. This is the process of bone formation. Also, in focusing on cells, they have cell-adhesive proteins called integrins on their surfaces. In these cells, the adhesion function of integrins would be carried out by peptide ligands [18]. Arg-Gly-Asp (RGD) is a type of peptide ligand that has been shown to promote osteoblast adhesion [19,20]. In the case of the RGD modified with hyaluronan, it has been reported to stimulate cell adhesion [21]. Glycine-histidine-lysine (GHK) is also the peptide ligand found in osteonectin that has been reported to enhance osteogenic differentiation [22]. Bioceramics that could facilitate this process have not yet been synthesized, which is a challenge in the development of synthetic bone.

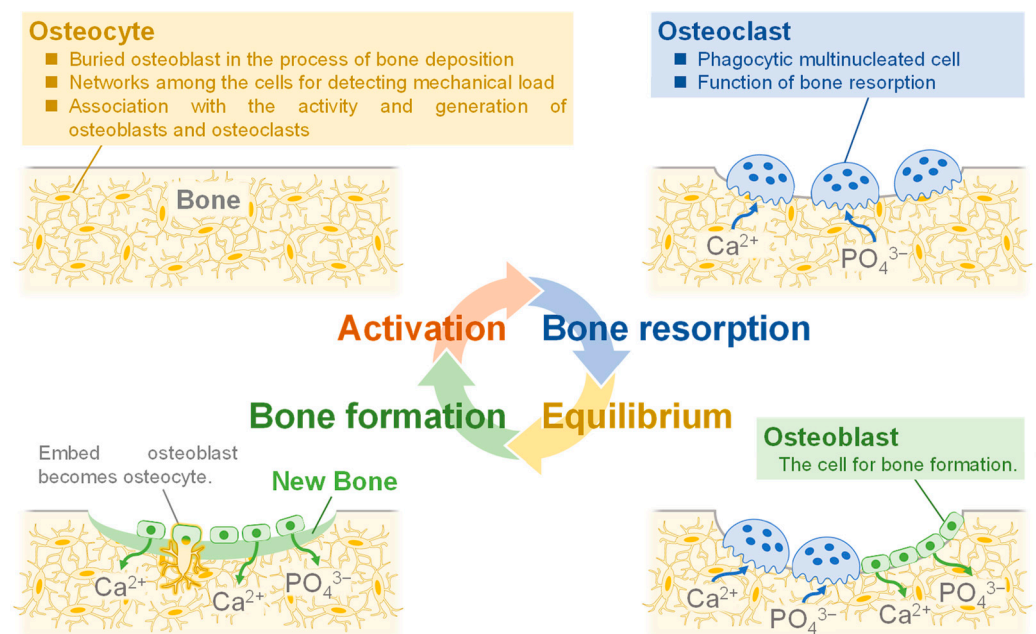


Figure 1. Illustration of the process of bone formation in vivo.

As mentioned above, for preparing specific materials that promote bone formation and are compatible with both bone replacement and therapy, the following conditions are required:

- (1) Bioceramics that resemble biological bone [23].
- (2) Bioceramics with low crystallinity [24].
- (3) Bioceramics of nanocrystalline structure [25–27].

Bioceramics that fulfil these conditions can be used to replace bone defects without toxicity to the bone, and their high bioactivity can elute bone-like components at the interface between the bone and the bioceramics to promote rapid adhesion between the bone and the bioceramics, thus facilitating treatment and allowing early treatment of bone defects [28].

In this review, the current status and issues of bone defect sites in the human body are explained based on examples of conventional HA, and the necessity of regenerative functions in addition to bone defect sites for biomedical applications is proposed. The characteristics and properties of HA substituted with heterogeneous ions such as silicate, carbonate, and other elemental ions are also explained. The importance of the surface characteristics of HA and its components, the hydration layers, and the non-apatitic layers for the effective control of biomedical function, as well as their relationship at the interface to improve biocompatibility, are highlighted. The possibility of a surface layer being formed between HA and its components is also proposed.

2. Hydroxyapatite (HA) Substituted with Other Ions

2.1. Characteristics of HA

CP is composed of Ca^{2+} and PO_4^{3-} or $\text{P}_2\text{O}_7^{4-}$ and is classified as a bioceramic. Table 1 shows the classification of CP compounds. It is classified according to the Ca/P molar ratio, which is the ratio of Ca^{2+} to PO_4^{3-} . Six types are present in hard tissues in vivo, with Ca/P molar ratios in the range of 1.0–1.67 [29]. The bioactivity of it is related to their crystalline structure, porosity, and dissolution rate, which are controlled by changing the parameters for various biomedical applications. In particular, the porosity of HA containing nanoparticles or nanopores is expected to function as a drug delivery system [30,31]. The controlled parameters are known to be dominantly influenced by the Ca/P molar ratio. Among the CPs, HA is the major component of bone and has been widely studied by controlling the parameters.

Table 1. Classification of the calcium phosphate compounds.

CP Compound	Abbreviation	Chemical Formula	Ca/P
Dicalcium phosphate dehydrate	DCPD	$\text{Ca}(\text{HPO}_4)_2 \cdot \text{H}_2\text{O}$	1.00
Octacalcium phosphate	OCP	$\text{Ca}_8\text{H}_2(\text{PO}_4)_6 \cdot 5\text{H}_2\text{O}$	1.33
Tricalcium phosphate	α -TCP β -TCP	$\text{Ca}_3(\text{PO}_4)_3$	1.50
Hydroxyapatite	HA	$\text{Ca}_{10}(\text{PO}_4)_6(\text{OH})_2$	1.67
Amorphous calcium phosphate	ACP	$\text{CaHPO}_4 \cdot n\text{H}_2\text{O}$	–

Figure 2 shows the crystalline structure of HA, with (a) the overall view and (b) the view from [001]. HA has a Ca/P molar ratio of 1.67 and a chemical composition of $\text{Ca}_{10}(\text{PO}_4)_6(\text{OH})_2$. The crystalline structure is hexagonal, the space group is $\text{P}6_3/\text{m}$, and the unit cell size is $a = 0.94$ nm and $c = 0.69$ nm. The calcium in the structure is classified into Ca(I) (columnar Ca) and Ca(II) (axis Ca), where the Ca(I) is aligned parallel to the c -axis and the Ca(II) surrounds the c -axis at the four corners of each unit cell where hydroxyl groups are present [32]. It is also known that HA has a high ion exchange capacity. The Ca^{2+} is substituted by Na^+ , K^+ , Mg^{2+} , etc.; the PO_4^{3-} by SiO_4^{4-} , CO_3^{2-} , etc.; and the OH^- by F^- , Cl^- , etc. [33]. These ions are thought to exist within the crystal and on the surface. They exist by substitution with Ca^{2+} , PO_4^{3-} , and/or OH^- when they are present inside the crystal and by reaction with functional groups such as P-OH and Ca-OH exposed on the surface when they are present on the surface.

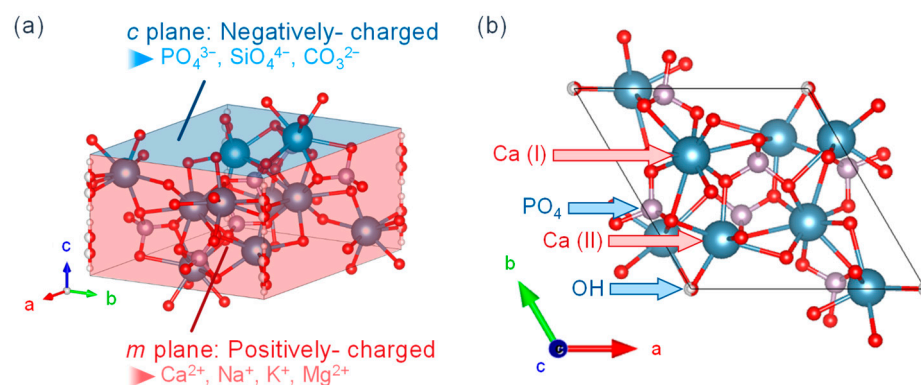


Figure 2. HA crystalline structure from the views of (a) overall and (b) [001].

Amorphous HA can be synthesized by some synthetic methods; highly crystalline and stable HA can be obtained by calcination of amorphous HA. HA is known to have high biocompatibility since it is contained in biological hard tissues. Therefore, it is used in biomaterials such as artificial bones and implants, and as a fixation layer for chromatography due to its high protein adsorption capacity [34–36]. Recently, its biocompatibility and protein adsorption capacity have been investigated for use as a drug delivery system [37,38].

The composition, structure, and morphology of HA vary greatly depending on the synthetic method. The techniques for synthesizing HA include the hydrothermal method, chemical precipitation method, emulsion method, and solid phase reaction method [39–43]. In human bodies, HA is synthesized by the biomineralization process. Recent studies on biomineralization described the biological formation of HA and its nucleation in body fluids to finally be self-assembled into complex structures such as teeth and bones [44]. The HA obtained by the biomineralization process promotes osteoblast adhesion, proliferation, and osseointegration [45,46]. The method for precipitating HA by simulating the biological fluid environment has been studied. Among these synthetic methods of producing HA, except for the hydrothermal method, calcium-deficient HA (CDHA) is easily obtained. Furthermore, ACP can be easily precipitated in aqueous solutions of Ca^{2+} and PO_4^{3-} at pH values above 9 for synthetic HA. The obtained ACP can be converted to HA by the recrystallization method [33,47,48].

2.2. Synthesis of HA to Enhance Its Biological Functions: Ion Substitution with Different Elements

HA in biological hard tissues is substituted with various elemental ions, such as carbonate and silicate ions, that work on the concentration, size, and type of action on the HA crystal lattice to enhance its physicochemical properties by altering its electron density and surface conditions [49]. Table 2 shows the different elemental ions that can be substituted in HA. These substitutions can be a cationic ion (with Ca^{2+}) or an anionic ion (with PO_4^{3-} and OH^-). Ionic substitution affects lattice parameters, crystallinity, surface charge, and morphology. The Ca^{2+} sites are mainly replaced by alkali metals and alkaline earth metals, and partially by transition metals. The lattice constants of the HA crystal structure are changed by these substitution ions, which is mainly attributed to the deficiency of OH^- and Ca^{2+} and the change of ionic radius. For example, Mg^{2+} , Sr^{2+} , Mn^{2+} , and Zn^{2+} ions increase the a-axis and the c-axis, while Na^+ , SiO_4^{4-} , CO_3^{2-} (type B), and F^- ions decrease the a-axis and increase the c-axis, CO_3^{2-} (type A) and Cl^- increase the a-axis and decrease the c-axis, and K^+ decreases the a and c-axis [49].

Table 2. Different ionic elements substituted into the HA structure for improving its functions.

Substitution Ion		Function
Cation	Na ⁺	Excellent osteoconductivity, improvement of cell proliferation
	K ⁺	Improvement of thermal stability
	Mg ²⁺	Enhancement of crystallization, crystal growth, thermal stability, influence on the dissolution
	Sr ²⁺	Inhibition of bone resorption, enhancement of bone formation
	Mn ²⁺	Cell adhesion activation
	Zn ²⁺	Enhancement of bone formation
Anion	SiO ₄ ⁴⁻	Enhancement of bioactivity, improvement of dissolution speed
	CO ₃ ²⁻	Higher specific surface area, lower crystallite size, excellent osteoconductive properties, higher solubility
	F ⁻	Higher stability, lower solubility, promotion of remineralization
	Cl ⁻	Excellent osteoconductive properties, higher solubility

The functions performed by the other elemental ions that are substituting in HA in biological bone affect various components of the bone metabolic process. The important phenomena in bone formation and implantation, namely osteoinduction, osteoconduction, and osseointegration, have been investigated in the previous study [50,51]. Osteoinduction is the process by which primitive, undifferentiated pluripotent cells are stimulated in some way to grow into the osteogenic cell lineage and induce osteogenesis [51,52]. In addition to osteoblasts and osteoclasts, the bones and surrounding tissues contain many undifferentiated cells. These undifferentiated cells have been reported to develop into osteocytes over time and are crucially important for bone healing and implant fixation [53]. The other elemental ions have been reported to promote bone formation and other processes by regulating the expression of genes and proteins involved in various stages of osteogenic differentiation [54–57]. This is a fundamental biological mechanism that occurs regularly in bone defect treatment and implantation. Osteoconduction refers to the ability of biomaterial surfaces to grow bone and is the process of inducing the adaptation of different biomaterial surfaces to the biological body. Since bone growth at the implant surface is dependent on the action of differentiated osteocytes, it can be considered that osteoconduction is dependent on osteoinduction. Moreover, various types of bone growth factors are required for bone formation and bone growth, including osteoconduction, which cannot occur without an adequate blood supply [58]. Osteoconduction in implants also depends on the biomaterial used and its response. In the case of metallic materials, there are reports showing that osteoconduction is not possible with Ag and Cu while it is possible with Ti and other materials [50]. Osseointegration is defined as the direct contact between bone and implant at the order-level by an optical microscope, as well as between the implant and bone via the cells or other biological tissues, with the result that the bone tissue can be formed at the bone-implant interface and the implant is directly fixed [59,60]. Osseointegration is not an isolated phenomenon; it depends on bone induction and osteogenesis. Therefore, materials that cannot promote bone growth cannot undergo osseointegration. These phenomena are interrelated, and the development of biomaterials that contribute to these phenomena is considered very important in the field of implants.

The substitution of other elemental ions in HA can enhance osteoblast differentiation, osteoinductive, osteoconductive, and osseointegration functions, such as the release of substituted ions due to reduced solubility of HA. Substitution of Cu²⁺, Mg²⁺, and SiO₄⁴⁻ enhances osteoinduction, whereas substitution of Na⁺, CO₃²⁻, and Cl⁻ enhances osteoinduction [61–63]. Furthermore, HA substituted with Zn²⁺ and Sr²⁺ has various biological functions, such as enhancement of bone formation and suppression of bone resorption and osteoporosis. It has been reported that SiO₄⁴⁻-substituted HA improves osseointegration properties and dissolution rate. F⁻-substituted HA was used to treat osteoporosis; however, excessive amounts of F⁻ may cause osteosclerosis and other diseases [64–70]. The combination of these different elemental ion substitutions is considered important for the synthesis of HA, which retains its beneficial properties for bone formation.

2.3. Structure and Properties of HA with Silicate Ion Substitution

Studies have found that the human body contains about 1–2 g of silicon (Si), and biological bone contains 36 ppm [71,72]. In mice and rats, 0.5 wt.% Si is present in the active growth points of bones [73], and a lack of Si in the diets of mice and rats leads to abnormal bone growth and cranial deformation [74]. The presence of Si affects bone growth. In vitro studies demonstrated that the ingestion of Si, in the form of orthosilicate, enhanced collagen I synthesis and promoted osteoblast differentiation [75]. On the other hand, in synthetic bioactive ceramics, such as bio-glasses and apatite-wollastonite containing SiO_2 , the reactivity of the crystalline surface containing Si affects its bioactivity [76]. SiO_4^{4-} -substituted HA particles have also been produced in various forms and used as coatings for titanium implants, showing improved osseointegration properties [66,68,77]. A synthetic porous SiO_4^{4-} -substituted HA with the trade name Actifuse TM has been successfully used as a bone replacement material in patients with level 1–2 lumbar degenerative disease and was found to be as effective as an autologous bone graft [78]. Figure 3 shows the crystal structures of previously described SiO_4^{4-} -substituted HA [76]. Silicic acid was present in HA in the form of an anionic substitution. Gibson et al. successfully synthesized the single-phase SiO_4^{4-} -substituted HA with SiO_4^{4-} substitution (0.4 wt.%) into the PO_4^{3-} site of HA with a precipitation reaction using calcium hydroxide as the calcium source, orthophosphoric acid as the phosphoric acid source, and silicon tetraacetate as the SiO_4^{4-} source. The compositional formula was proposed as shown in Equation (1) [76].

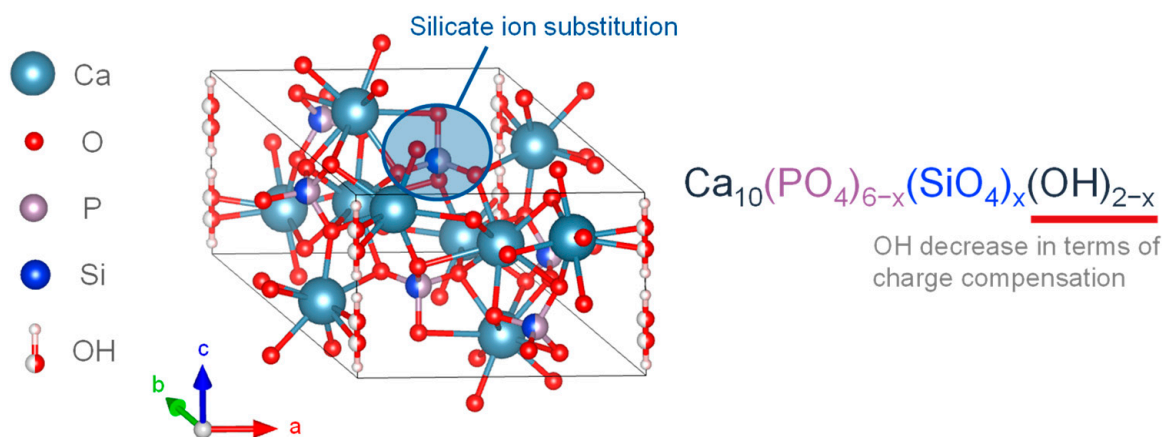
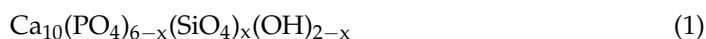


Figure 3. Silicon-substituted HA crystalline structure.

The experimental results of SiO_4^{4-} substitution of HA showed that the OH^- group decreased with the SiO_4^{4-} substitution, and the SiO_4^{4-} substitution caused changes in the crystal structure and chemical composition, including a decrease in the a -axis and an increase in the c -axis [76]. Bianco et al. synthesized SiO_4^{4-} -substituted α -TCP in a mixed phase with 1.26 wt.% SiO_4^{4-} and CO_3^{2-} with a precipitation reaction using calcium hydroxide as the calcium source, orthophosphoric acid as the phosphoric acid source, and tetraethoxysilane (TEOS) as the SiO_4^{4-} source. As a result, these particles were found to have an increased a -axis and c -axis [79]. In an example of synthesizing SiO_4^{4-} -substituted HA by varying the added amount of SiO_4^{4-} from 0.8–5.0 wt.%, it was confirmed that the incorporated concentration of SiO_4^{4-} was up to 1.5 wt.%, and the SiO_4^{4-} -substituted HA exceeding 1.5 wt.% contained ACP with amorphous silica [80].

2.4. Structures and Properties of Carbonate Ion Substituted HA

Carbonate ion (CO_3^{2-}) is present in biological hard tissues, such as biological bone and dentin tissue, in an amount of 2.3–8.0 wt.%, in the form of substitution with PO_4^{3-} and OH^- in HA [81,82]. The crystalline structure of CO_3^{2-} -substituted HA is similar to

that of HA in biological hard tissues. It is suggested to play an important role in bone metabolism and is expected to be used as a bone replacement material [81–85].

Figure 4 shows the crystalline structure of two types of CO_3^{2-} -substituted HA. It is an anionic substitution and has two different forms depending on the substitution site [86–88]. The A-type carbonate HA is in Figure 4a. It is called carbonate apatite (CAP), and is the substitution form in which CO_3^{2-} is substituted with the OH site of HA. The chemical composition is expressed by the formula in Equation (2).

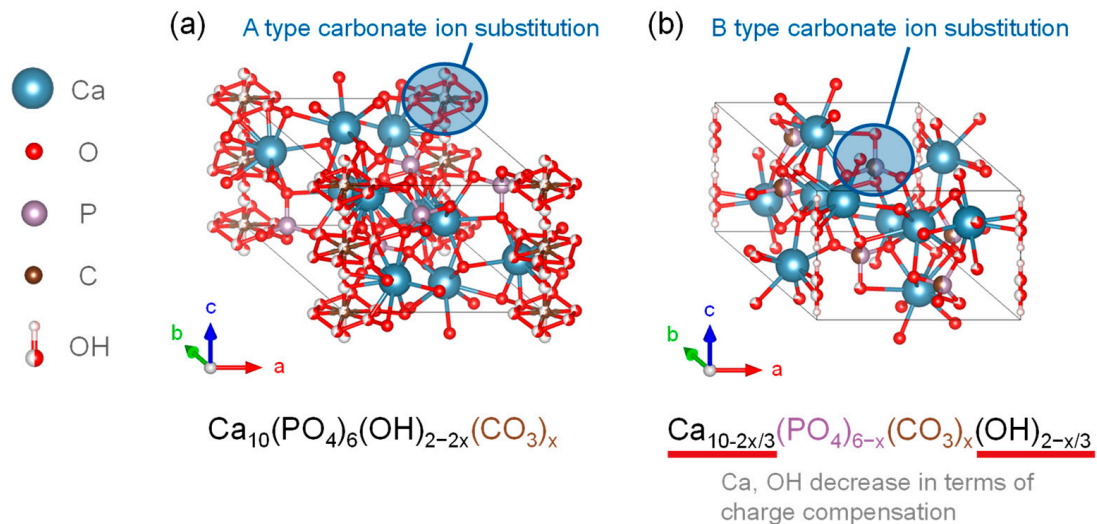
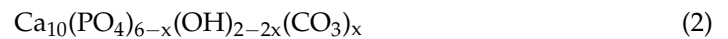
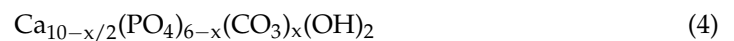
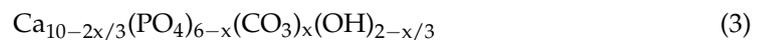


Figure 4. Carbonate-substituted hydroxyapatite crystalline structures of (a) CAP and (b) CHA.

In general, CAP can be synthesized by heating HA to approximately 1000 °C in a carbon dioxide atmosphere [89]. The lattice parameters of CAP prepared by Walleyes showed an increase in the a -axis and a decrease in the c -axis in X-ray diffraction. It was reported that for every 1 wt.% substitution of CO_3^{2-} in CAP, the a -axis of the lattice parameter was lengthened by 0.0025 nm, with an upper limit of up to 4.4 wt.% [90,91].

The B-type carbonate-substituted HA (CHA) shown in Figure 4b is a substitutional form in which CO_3^{2-} was substituted at the PO_4^{3-} site of HA, and the chemical compositions of the substitutional formulas are given in Equations (3) and (4) [92].



CHA remains charge neutral due to the loss of Ca^{2+} and OH^- upon CO_3^{2-} substitution. For each 1 wt.% substitution of CO_3^{2-} , the a -axis of the lattice parameter was shortened by 0.00006 nm and the c -axis was elongated, which could be up to the maximum inclusion content of 22.2 wt.% [91]. The AB-type carbonate-ion-substituted HA, in which carbonate ions were substituted at both the PO_4^{3-} and OH^- sites of the HA crystalline structure, was also present [93]. The HA showed enhanced dissolution properties in vitro and in vivo, and had higher osteoconductivity than the stoichiometric HA. The increased CO_3^{2-} content in HA results in the formation of CaO and β -TCP phases by calcination at temperatures where CO_3^{2-} decomposes, and the mechanical tests showed that CAP had similar strength to that of stoichiometric HA [93].

In dentistry, it was observed that an increase in CO_3^{2-} content increases the dissolution characteristics of HA in weak acids. This property has been reported to preferentially dissolve tooth enamel, the surface material of teeth, in the initial stages of dental caries, lead-

ing to the progression of caries [94,95]. Depending on the progression of caries, secondary caries and tooth erosion may occur; therefore, proper control of CO_3^{2-} ion substitution is important [96,97]. Thus, the changes caused by HA dissolution in bone due to CO_3^{2-} ions should be studied from the viewpoints related to bone remodelling.

3. Surface Layers on HA

3.1. Hydration Layer

As the bioceramics come into the contact with water molecules, the water molecules are adsorbed onto the surfaces and the hydration layers are formed. The formation of the hydration layer is caused by various factors, including the interactions between the bioceramic surfaces, ions, and water molecules. The interactive states play an essential role in the subsequent biological reactions [98–100].

Figure 5 shows the three hydration layers on the bioceramic surface. In most of the studies, the hydration layer consists of three layers: unfrozen water, intermediate water, and free water, and it has been thought that the cell-adhesive proteins are affected by retaining these layers [101]. Non-freezing and intermediate water are unable to form hydrogen bonds due to strong interactions with the bioceramic surface, thus, water molecules remain in a state where they can move and are difficult to freeze. Free water does not directly interact with the bioceramic surfaces and behave similarly to bulk water, forming hydrogen bonds with the surrounding H_2O . Below $0\text{ }^\circ\text{C}$ it freezes, thus stopping the molecular motion. The difference between the three layers was evaluated in terms of the heat balance during the freezing and melting of water by differential scanning calorimetry (DSC) and the mobility of water molecules by $^1\text{H-NMR}$ [102]. The difference between the three layers was due to their interaction acting on the bioceramic surfaces, which modifies the melting point and the mobility. Based on the thermal value at each transition of DSC, non-freezing water was defined as water that does not freeze at $-100\text{ }^\circ\text{C}$; intermediate water was water that froze at temperatures lower than $0\text{ }^\circ\text{C}$ during the temperature increase process; and free water was water that froze at temperatures below $0\text{ }^\circ\text{C}$ and crystallized at $-100\text{ }^\circ\text{C}$ [102]. The layer structure was defined as water that was crystallized at temperatures below $0\text{ }^\circ\text{C}$ and crystallizes at $-100\text{ }^\circ\text{C}$ [103]. The structure of the hydration layer rearranges on femto- to picosecond time scales, and liquid water is an amorphous structure with a disordered network on very short time scales; however, it has the randomness of a liquid on longer time scales. In $^1\text{H-NMR}$ measurements, the relaxation times of non-freezing water, intermediate water, and free water were 10^{-8} – 10^{-6} s, 10^{-10} – 10^{-9} s, and 10^{-12} – 10^{-11} s, respectively, indicating stronger interactions with the bioceramics as well as lower mobility [102]. In the FT-IR spectra, the layer state could be evaluated by separating the absorption bands of the stretching vibration of the hydroxyl groups (3600 cm^{-1} , 3400 cm^{-1} , 3200 cm^{-1}) corresponding to non-freezing water, intermediate water, and free water, respectively [102]. A variety of other analytical methods were used to evaluate the hydration structure (i.e., hydrogen molecular bonding state and mobility). However, the layer on the HA surface has not been studied in detail, thus it is necessary to evaluate the layer bonded to the surface as an integral part.

3.2. Non-Apatitic Layer on HA Surface

Figure 6 shows a model of the surface layer bounded with the HA. Biological apatite in naturally calcified tissue is formed *in vivo* in an aqueous environment at room temperature. Thus, recent studies of HA have focused on HA prepared by wet methods, which can synthesize HA similar to the *in vivo* environment in order to mimic biological apatite. The detailed surface structure of the HA synthesized by wet methods has not been fully elucidated; however, it is predicted that it will be a low-crystalline surface, and such a structure is being studied by spectroscopic methods such as FT-IR and NMR, which are sensitive to perturbations of the local ionic environment. FT-IR spectra show an absorption band in the 680 – 480 cm^{-1} region corresponding to the non-apatitic layer on the HA surface, which is assigned to PO_4^{3-} and HPO_4^{2-} [103]. The coordination environment of phosphate

and calcium ions and the interaction of these ions were investigated by NMR spectroscopy, indicating that the HA particles are composed of a highly crystalline core and a non-apatite layer composed of ACP [104]. The layer is highly reactive due to its unstable structure composed of divalent ions such as Ca^{2+} , HPO_4^{2-} , and CO_3^{2-} , etc. In particular, it has been shown from ab initio calculations that the reaction with H_2O exhibits moderate Lewis acidity due to the strong bonding of the exposed ions in the non-apatitic layer (e.g., Ca^{2+} , HPO_4^{2-} , CO_3^{2-} , etc.) due to electrostatic interactions with the H_2O [105,106]. The ions in the layer are organized in a geometric configuration and are stabilized by a structured hydrogen bonding network of the hydration layer [106]. In addition to this reaction, the layer is believed to contribute to the growth of HA nuclei, ion exchange, and the adsorption of organic molecules. The reactivity of the layer is thought to play a significant role in biocompatibility, and further research is needed.

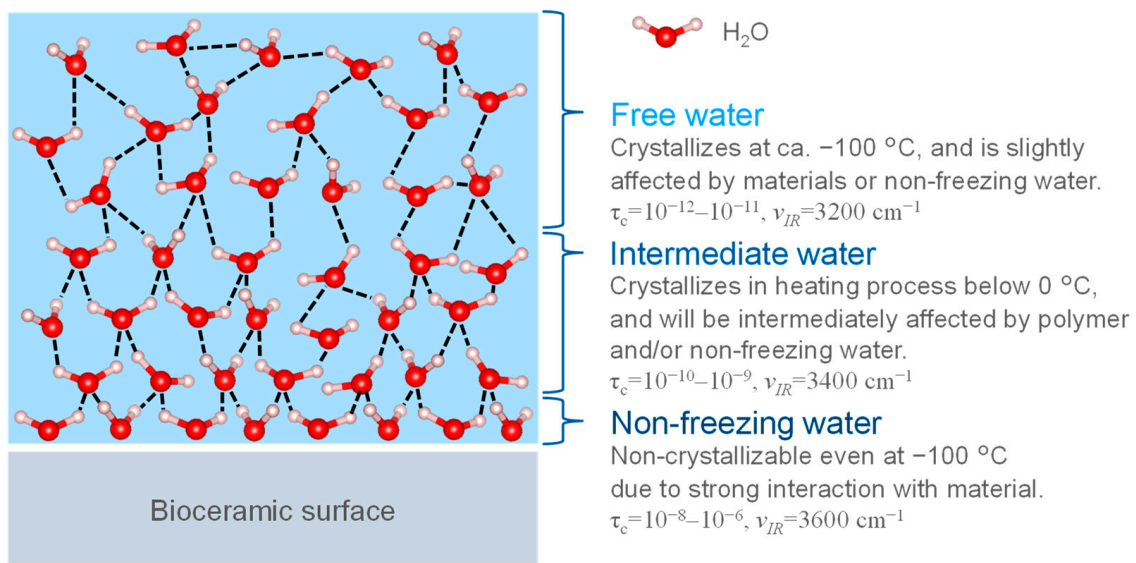


Figure 5. The three types of hydration layers. τ_c : relaxation time of water molecule motion by solid state NMR measurement. ν_{IR} : IR absorption wavenumber.

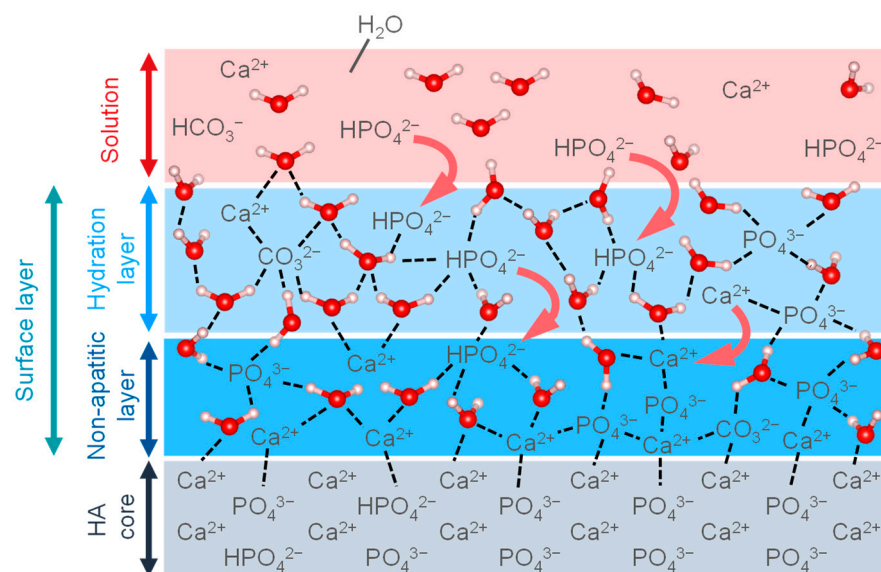


Figure 6. Illustration of the surface layers on HA core.

3.3. Relationship between the Surface Layer and Biocompatibility

The biocompatibility of HA is highly related to the cell adhesion behavior, and the cell-bioceramic interfaces are formed *in vivo*, as shown in Figure 7 [107,108]. Firstly, the cell adhesion occurs through three processes upon implantation in the body. In the process, H₂O and ions in body fluid adsorb on the surfaces, forming the hydration layer. Here, the amount of H₂O, the concentration and type of ions in the vicinity of the bioceramics are important factors for the next processes. In the second process, the proteins are adsorbed onto the hydration layer, and the protein adsorption is saturated to form the protein adsorption layer. The type and orientation structure of the adsorbed protein in this process determine the function of the attached cells. In the third process, the cells are adhered to the adsorbed protein layer and proliferate with their spreading. The layers formed by the first and second processes determine the cell behavior. Thus, it is important to control the first process and then evaluate the protein adsorption layer for the desired cell adhesion properties in order to consider biocompatibility [109,110]. The highly-reactive surface layer on HA is known to interact strongly with the substances in surrounding aqueous solutions [111–113]. The interactions are supported by ion mobility, ion exchange capacity, and molecular adsorption [114–116]. The interfacial phenomena induce the combination between HA surface layer and water, such as the dissolution and deposition of ions and the solid dissolution of organic and mineral phases [117–119]. In other words, the interfacial phenomena are considered to be the formation process of the HA surface layer that affects the hydration layer and cell adhesion. In particular, the inclusion of SiO₄⁴⁻ and CO₃²⁻ ions in HA induces structural defects and increases its dissolution rate *in vivo* [120–122]. This promotes hydrogen bonding networks, increases cell and bone attachment rates, and activates osteoblasts, leading to the activation of surrounding tissues based on increased rates of ion solubilization and diffusion. This phenomenon is related to the ion exchange behavior at the non-apatitic layer of the HA surface, where the other elemental ions that have leached and diffused into the layer by the ion exchange increase the genetic markers and proteins for inducing osteogenesis, and some reports suggest the increase in the activity of osteoblasts [54–58]. These surface phenomena of ion-substituted HA affect the hydration layer, leading to significant changes in the dissolution properties of HA and contributing to its biocompatibility, resulting in improved protein adsorption, cell adhesion, and osteogenesis.

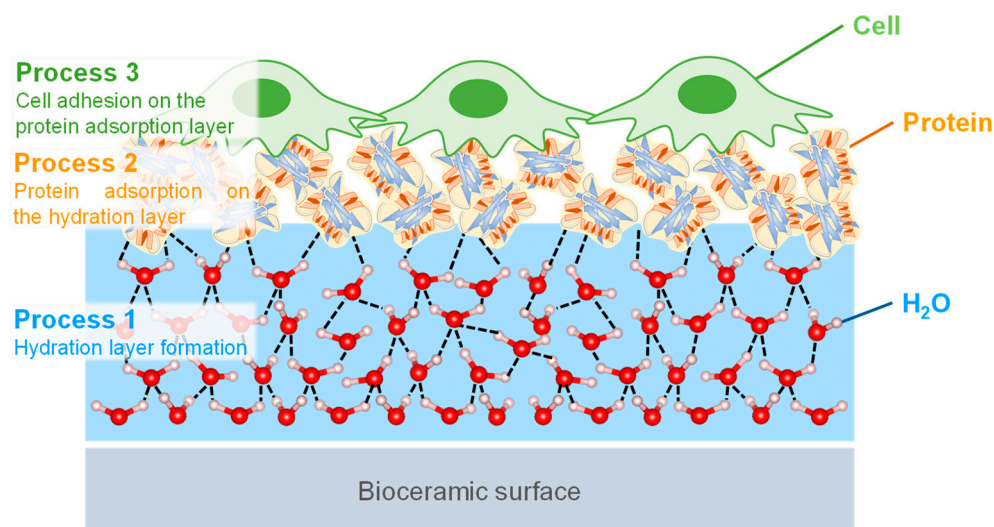


Figure 7. Illustration of the cell adhesion processes of (1) the hydration layer formed on the bioceramic surface, (2) protein adsorption on the hydration layer, and (3) cells that recognize and adhere to the protein adsorption layer.

4. Conclusions

In this review, the current status of the effect of substitution ions on the surface properties and biocompatibility of HA was discussed. Changing the chemical composition and crystalline structure of HA depending on the synthesis method and added ions was emphasized, which improved the surface properties of HA and thus affected its biocompatibility. In particular, the ability of HA to be substituted by silicate and carbonate is remarkable for its use as a bioceramic. Furthermore, the characteristics of the HA surface layers (i.e., hydrated and non-apatite layers) that affect subsequent biological responses were clearly summarized and categorized. Since the surface layers are important for both protein adsorption and cell adhesion, analysis of their properties may provide important clues to gain insight into the efficient mechanisms of bone formation.

Author Contributions: Writing of the manuscript, K.S.; review and editing, Y.Z., T.G.P.G. and R.K.; supervision, M.T. All authors have read and agreed to the published version of the manuscript.

Funding: This research received no external funding.

Institutional Review Board Statement: Not applicable.

Data Availability Statement: Not applicable.

Conflicts of Interest: The authors declare no conflict of interest.

References

1. Bauer, T.W.; Muschler, G.F. Bone Graft Materials. *Clin. Orthop. Relat. Res.* **2000**, *371*, 10–27. [[CrossRef](#)]
2. Younger, E.M.; Chapman, M.W. Morbidity at Bone Graft Donor Sites. *J. Orthop. Trauma* **1989**, *3*, 192–195. [[CrossRef](#)] [[PubMed](#)]
3. Banwart, J.C.; Asher, M.A.; Hassanein, R.S. Iliac Crest Bone Graft Harvest Donor Site Morbidity. *Spine* **1995**, *20*, 1055–1060. [[CrossRef](#)] [[PubMed](#)]
4. Arrington, E.D.; Smith, W.J.; Chambers, H.G.; Bucknell, A.L.; Davino, N.A. Complications of iliac crest bone graft harvesting. *Clin. Orthop. Relat. Res.* **1996**, *329*, 300–309. [[CrossRef](#)] [[PubMed](#)]
5. Greenwald, A.S.; Boden, S.D.; Goldberg, V.M.; Khan, Y.; Laurencin, C.T.; Rosier, R.N. Bone-Graft Substitutes: Facts, Fictions, and Applications. *J. Bone Jt. Surg.* **2001**, *83*, 98–103. [[CrossRef](#)]
6. Wu, S.; Liu, X.; Yeung, K.W.K.; Liu, C.; Yang, X. Biomimetic porous scaffolds for bone tissue engineering. *Mater. Sci. Eng. R Rep.* **2014**, *80*, 1–36.
7. Zwingerberger, S.; Nich, C.; Valladares, R.D.; Yao, Z.; Stiehler, M.; Goodman, S.B. Recommendations and Considerations for the Use of Biologics in Orthopedic Surgery. *BioDrugs* **2012**, *26*, 245–256.
8. Guyton, A.C.; Hall, J.E. *Text Book of Medical Physiology (Guyton Physiology)*, 11th ed.; Elsevier: Amsterdam, The Netherlands, 2006.
9. Parfitt, A.M. Osteonal and hemi-osteonal remodeling: The spatial and temporal framework for signal traffic in adult human bone. *J. Cell. Biochem.* **1994**, *55*, 273–286. [[CrossRef](#)]
10. Aarden, E.M.; Nijiwede, P.J.; Burger, E.H. Function of osteocytes in bone. *J. Cell. Biochem.* **2003**, *55*, 287–299. [[CrossRef](#)]
11. Bonewald, L.F. The Amazing Osteocyte. *J. Bone Miner. Res.* **2010**, *26*, 229–238. [[CrossRef](#)]
12. Bellido, T. Osteocyte-Driven Bone Remodeling. *Calcif. Tissue Int.* **2014**, *94*, 25–34. [[CrossRef](#)]
13. Teitelbaum, S.L. Bone Resorption by Osteoclasts. *Science* **2000**, *289*, 1504–1508. [[CrossRef](#)] [[PubMed](#)]
14. Blair, H.C. How the osteoclast degrades bone. *BioEssays* **1998**, *20*, 837–846. [[CrossRef](#)]
15. Anderson, H.C. Mechanism of mineral formation in bone. *Lab. Investig.* **1989**, *60*, 320–330. [[PubMed](#)]
16. Cölfen, H. A crystal-clear view. *Nat. Mater.* **2010**, *9*, 960–961. [[CrossRef](#)] [[PubMed](#)]
17. Golub, E.E. Role of matrix vesicles in biomineralization. *Biochim. Biophys. Acta-Gen. Subj.* **2009**, *1790*, 1592–1598.
18. Pierschbacher, M.D.; Ruoslahti, E. Cell attachment activity of fibronectin can be duplicated by small synthetic fragments of the molecule. *Nature* **1984**, *309*, 30–33. [[CrossRef](#)]
19. Schaffner, P.; Dard, M.M. Structure and function of RGD peptides involved in bone biology. *Cell. Mol. Life Sci.* **2003**, *60*, 119–132. [[CrossRef](#)] [[PubMed](#)]
20. Anselme, K. Osteoblast adhesion to biomaterials. *Biomaterials* **2000**, *21*, 667–681.
21. Balasundaram, G.; Sato, M.; Webster, T.J. Using hydroxyapatite nanoparticles and decreased crystallinity to promote osteoblast adhesion similar to functionalizing with RGD. *Biomaterials* **2006**, *27*, 2798–2805. [[CrossRef](#)]
22. Klontzas, M.E.; Reakasame, S. Oxidized alginate hydrogels with the GHK peptide enhance cord blood mesenchymal stem cell osteogenesis: A paradigm for metabolomics-based evaluation of biomaterial design. *Acta Biomater.* **2019**, *88*, 224–240. [[CrossRef](#)]
23. Ogiso, M.; Kaneda, H.; Arasaki, J.; Ishida, K.; Tabata, T. Epithelial attachment to hydroxyapatite ceramics implant. *J. Dent. Res.* **1980**, *59*, 941.
24. Koutsopoulos, S. Synthesis and characterization of hydroxyapatite crystals: A review study on the analytical methods. *J. Biomed. Mater. Res.* **2002**, *62*, 600–612. [[CrossRef](#)] [[PubMed](#)]

25. Stupp, S.I.; Ciegler, G.W. Organoapatites: Materials for artificial bone. I. Synthesis and microstructure. *J. Biomed. Mater. Res.* **1992**, *26*, 169–183. [[CrossRef](#)] [[PubMed](#)]
26. Webster, T. Enhanced osteoclast-like cell functions on nanophase ceramics. *Biomaterials* **2001**, *22*, 1327–1333. [[CrossRef](#)] [[PubMed](#)]
27. Huang, J.; Best, S.M.; Bonfield, W.; Brooks, R.A.; Rushton, N.; Jayasinghe, S.N.; Edirisinghe, M.J. In vitro assessment of the biological response to nanosized hydroxyapatite. *J. Mater. Sci. Mater. Med.* **2004**, *15*, 441–445. [[CrossRef](#)] [[PubMed](#)]
28. Mocquot, C.; Attik, N.; Pradelle-Plasse, N.; Grosogeat, B.; Colon, P. Bioactivity assessment of bioactive glasses for dental applications: A critical review. *Dent. Mater.* **2020**, *36*, 1116–1143. [[CrossRef](#)]
29. Tung, M.S. Calcium Phosphates: Structure, Composition, Solubility, and Stability. In *Calcium Phosphates in Biological and Industrial Systems*; Springer: Berlin/Heidelberg, Germany, 1998; pp. 1–19.
30. Munir, M.U.; Salman, S. Nano-hydroxyapatite as a delivery system: Overview and advancements. *Artif. Cells Nanomed. Biotechnol.* **2021**, *49*, 717–727. [[CrossRef](#)]
31. Salètes, M.; Vartin, M.; Mocquot, C.; Chevalier, C.; Grosogeat, B.; Colon, P.; Attik, N. Mesoporous Bioactive Glasses Cytocompatibility Assessment: A Review of In Vitro Studies. *Biomimetics* **2021**, *6*, 9. [[CrossRef](#)]
32. Kay, M.I.; Young, R.A.; Posner, A.S. Crystal Structure of Hydroxyapatite. *Nature* **1964**, *204*, 1050–1052. [[CrossRef](#)]
33. Elliott, J.C. *Structure and Chemistry of the Apatites and Other Calcium Orthophosphates*; Elsevier: Amsterdam, The Netherlands, 1994.
34. Brown, W.E.; Eidelman, N.; Tomazic, B. Octacalcium Phosphate as a Precursor in Biomineral Formation. *Adv. Dent. Res.* **1987**, *1*, 306–313. [[CrossRef](#)] [[PubMed](#)]
35. Kawasaki, T. Theory of chromatography on hydroxyapatite columns with small loads. *J. Chromatogr. A* **1978**, *157*, 7–42. [[CrossRef](#)]
36. Otsuka, M.; Matsuda, Y.; Yu, D.; Wong, J.; Fox, J.L.; Higuchi, W.I. A novel skeletal drug delivery system for anti-bacterial drugs using self-setting hydroxyapatite cement. *Chem. Pharm. Bull.* **1990**, *38*, 3500–3502. [[CrossRef](#)] [[PubMed](#)]
37. Shinto, Y.; Uchida, A.; Korkusuz, F.; Araki, N.; Ono, K. Calcium hydroxyapatite ceramic used as a delivery system for antibiotics. *J. Bone Jt. Surg. Br.* **1992**, *74-B*, 600–604. [[CrossRef](#)]
38. Treboux, G.; Kanzaki, N.; Onuma, K.; Ito, A. Energy-Preeminent Isomer of the $\text{Ca}_3(\text{PO}_4)_2$ Cluster. *J. Phys. Chem. A* **1999**, *103*, 8118–8120. [[CrossRef](#)]
39. Feng, W.; Mu-sen, L.; Yu-peng, L.; Yong-xin, Q. A simple sol–gel technique for preparing hydroxyapatite nanopowders. *Mater. Lett.* **2005**, *59*, 916–919. [[CrossRef](#)]
40. Kuriakose, T.A.; Kalkura, S.N.; Palanichamy, M.; Arivuoli, D.; Dierks, K.; Bocelli, G.; Betzel, C. Synthesis of stoichiometric nano crystalline hydroxyapatite by ethanol-based sol–gel technique at low temperature. *J. Cryst. Growth* **2004**, *263*, 517–523. [[CrossRef](#)]
41. Liu, J.; Ye, X.; Wang, H.; Zhu, M.; Wang, B.; Yan, H. The influence of pH and temperature on the morphology of hydroxyapatite synthesized by hydrothermal method. *Ceram. Int.* **2003**, *29*, 629–633. [[CrossRef](#)]
42. Wang, P.; Li, C.; Gong, H.; Jiang, X.; Wang, H.; Li, K. Effects of synthesis conditions on the morphology of hydroxyapatite nanoparticles produced by wet chemical process. *Powder Technol.* **2010**, *203*, 315–321. [[CrossRef](#)]
43. Bose, S.; Saha, S.K. Synthesis and Characterization of Hydroxyapatite Nanopowders by Emulsion Technique. *Chem. Mater.* **2003**, *15*, 4464–4469. [[CrossRef](#)]
44. Dorozhkin, S.V. Nanometric calcium orthophosphates (CaPO_4): Preparation, properties and biomedical applications. *Adv. Nano-BioMater. Devices* **2019**, *3*, 422–513.
45. Cai, Y.; Liu, Y.; Yan, W.; Hu, Q.; Tao, J.; Zhang, M.; Shi, Z.; Tang, R. Role of hydroxyapatite nanoparticle size in bone cell proliferation. *J. Mater. Chem.* **2007**, *17*, 3780–3787. [[CrossRef](#)]
46. Mondal, S.; Maharta, S.; Kundu, S.; Mondal, B.I. Development of biocompatible sinterable hydroxyapatite from fish scale. *Mater. Sci. Eng.* **2007**, *C27*, 441–449.
47. LeGeros, R.Z. Calcium phosphates in oral biology and medicine. *Monogr. Oral Sci.* **1991**, *15*, 154–171.
48. Dorozhkin, S.V. Calcium Orthophosphate Bioceramics. *Eurasian Chem. J.* **2010**, *12*, 247. [[CrossRef](#)]
49. Ratnayake, J.T.B.; Mucalo, M.; Dias, G.J. Substituted hydroxyapatites for bone regeneration: A review of current trends. *J. Biomed. Mater. Res. Part B Appl. Biomater.* **2017**, *105*, 1285–1299.
50. Johansson, C.B.; Han, C.H.; Wennerberg, A.; Albrektsson, T. A Quantitative Comparison of Machined Commercially Pure Titanium and TitaniumAluminum-Vanadium Implants in Rabbit Bone. *Int. J. Oral Maxillofac. Implant.* **1998**, *13*, 315–321.
51. Albrektsson, T.; Johansson, C. Osteoinduction, osteoconduction and osseointegration. *Eur. Spine J.* **2001**, *10*, S96–S101.
52. Bruder, S.R.; Jaiswal, N.; Ricalton, N.S.; Mosca, J.D.; Kraus, K.H.; Kadiyala, S. Mesenchymal Stem Cells in Osteobiology and Applied Bone Regeneration. *Clin. Orthop. Relat. Res.* **1998**, *355*, S247–S256. [[CrossRef](#)]
53. Young, R.W. Nucleic acids, protein synthesis and bone. *Clin. Orthop. Relat. Res.* **1963**, *26*, 147–160. [[CrossRef](#)]
54. Jung, G.Y.; Park, Y.J.; Han, J.S. Effects of HA released calcium ion on osteoblast differentiation. *J. Mater. Sci. Mater. Med.* **2010**, *21*, 1649–1654. [[CrossRef](#)]
55. Wang, Y.; Zhang, S.; Zeng, X.; Ma, L.L.; Weng, W.; Yan, W.; Qian, M. Osteoblastic cell response on fluoridated hydroxyapatite coatings. *Acta Biomater.* **2007**, *3*, 191–197. [[CrossRef](#)]
56. Ni, G.X.; Yao, Z.P.; Huang, G.T.; Liu, W.G.; Lu, W.W. The effect of strontium incorporation in hydroxyapatite on osteoblasts in vitro. *J. Mater. Sci. Mater. Med.* **2011**, *22*, 961–967. [[CrossRef](#)]
57. Qi, T.; Weng, J.; Yu, F.; Zhang, W.; Li, G.; Qin, H.; Tan, Z.; Zeng, H. Insights into the Role of Magnesium Ions in Affecting Osteogenic Differentiation of Mesenchymal Stem Cells. *Biol. Trace Elem. Res.* **2021**, *199*, 559–567. [[CrossRef](#)] [[PubMed](#)]

58. Albrektsson, T. The healing of autologous bone grafts after varying degrees of surgical trauma. A microscopic and histochemical study in the rabbit. *J. Bone Jt. Surg. Br.* **1980**, *62-B*, 403–410. [[CrossRef](#)] [[PubMed](#)]
59. Albrektsson, T.; Brånemark, P.-I.; Hansson, H.-A.; Lindström, J. Osseointegrated Titanium Implants: Requirements for Ensuring a Long-Lasting, Direct Bone-to-Implant Anchorage in Man. *Acta Orthop. Scand.* **1981**, *52*, 155–170. [[CrossRef](#)] [[PubMed](#)]
60. Attik, N.; Phantarasmy, M.; Abouelleil, H.; Chevalier, C.; Barraco, A.; Grosgeat, B.; Lafon, A. Comparison of the Biological Behavior and Topographical Surface Assessment of a Minimally Invasive Dental Implant and a Standard Implant: An In Vitro Study. *Materials* **2022**, *15*, 7540. [[CrossRef](#)] [[PubMed](#)]
61. Cho, J.S.; Yoo, D.S.; Chung, Y.-C.; Rhee, S.-H. Enhanced bioactivity and osteoconductivity of hydroxyapatite through chloride substitution. *J. Biomed. Mater. Res. Part A* **2014**, *102*, 455–469. [[CrossRef](#)]
62. Veljovic, D.; Matic, T.; Stamenic, T.; Kojic, V.; Dimitrijevic-Brankovic, S.; Lukic, M.J.; Jevtic, S.; Radovanovic, Z.; Petrovic, R.; Janackovic, D. Mg/Cu co-substituted hydroxyapatite—Biocompatibility, mechanical properties and antimicrobial activity. *Ceram. Int.* **2019**, *45*, 22029–22039. [[CrossRef](#)]
63. Xu, T.; He, X.; Chen, Z.; He, L.; Lu, M.; Ge, J.; Weng, J.; Mu, Y.; Duan, K. Effect of magnesium particle fraction on osteoinduction of hydroxyapatite sphere-based scaffolds. *J. Mater. Chem. B* **2019**, *7*, 5648–5660. [[CrossRef](#)]
64. Bigi, A.; Boanini, E.; Capuccini, C.; Gazzano, M. Strontium-substituted hydroxyapatite nanocrystals. *Inorg. Chim. Acta* **2007**, *360*, 1009–1016. [[CrossRef](#)]
65. Gerstenfeld, S.; Hinojosa, L.; JL, F.M.; Marchante, J.M.; JL, G.A.; Sanz-Medel, A.; JB, C.A. Effect of strontium on bone metabolism in hemodialysis patients. *Nefrologia* **2003**, *23* (Suppl. S2), 52–56. [[PubMed](#)]
66. Kishi, S.; Yamaguchi, M. Inhibitory effect of zinc compounds on osteoclast-like cell formation in mouse marrow cultures. *Biochem. Pharmacol.* **1994**, *48*, 1225–1230. [[CrossRef](#)]
67. Baeza, A.; Izquierdo-Barba, I.; Vallet-Regí, M. Biotinylation of silicon-doped hydroxyapatite: A new approach to protein fixation for bone tissue regeneration. *Acta Biomater.* **2010**, *6*, 743–749. [[CrossRef](#)] [[PubMed](#)]
68. Hahn, B.D.; Lee, J.M.; Park, D.S.; Choi, J.J.; Ryu, J.; Yoon, W.H.; Lee, B.K.; Shin, D.S.; Kim, H.E. Aerosol deposition of silicon-substituted hydroxyapatite coatings for biomedical applications. *Thin Solid Film.* **2010**, *518*, 2194–2199. [[CrossRef](#)]
69. Cheng, K.; Shen, G.; Weng, W.; Han, G.; Ferreira, J.M.; Yang, J. Synthesis of hydroxyapatite/fluoroapatite solid solution by a sol-gel method. *Mater. Lett.* **2001**, *51*, 37–41. [[CrossRef](#)]
70. Porter, A.E.; Patel, N.; Skepper, J.N.; Best, S.M.; Bonfield, W. Effect of sintered silicate-substituted hydroxyapatite on remodelling processes at the bone-implant interface. *Biomaterials* **2004**, *25*, 3303–3314. [[CrossRef](#)]
71. Jugdaohsingh, R. Silicon and bone health. *J. Nutr. Health Aging* **2007**, *11*, 99–110.
72. Whiting, S.J.; Draper, H.H. Effect of a Chronic Acid Load as Sulfate or Sulfur Amino Acids on Bone Metabolism in Adult Rats. *J. Nutr.* **1981**, *111*, 1721–1726. [[CrossRef](#)]
73. Carlisle, E.M. Silicon as an essential trace element in animal nutrition. *Ciba Found. Symp.* **1986**, *121*, 123–139.
74. Carlisle, E.M. Silicon: An Essential Element for the Chick. *Science* **1972**, *178*, 619–621. [[CrossRef](#)]
75. Reffitt, D.M.; Ogston, N.; Jugdaohsingh, R.; Cheung, H.F.J.; Evans, B.A.J.; Thompson, R.P.H.; Powell, J.J.; Hampson, G.N. Orthosilicic acid stimulates collagen type 1 synthesis and osteoblastic differentiation in human osteoblast-like cells in vitro. *Bone* **2003**, *32*, 127–135. [[CrossRef](#)] [[PubMed](#)]
76. Gibson, I.R.; Best, S.M.; Bonfield, W. Chemical characterization of silicon-substituted hydroxyapatite. *J. Biomed. Mater. Res.* **1999**, *44*, 422–428.
77. Li, D.-H.; Lin, J.; Lin, D.-Y.; Wang, X.-X. Synthesized silicon-substituted hydroxyapatite coating on titanium substrate by electrochemical deposition. *J. Mater. Sci. Mater. Med.* **2011**, *22*, 1205–1211. [[CrossRef](#)]
78. Jenis, L.G.; Banco, R.J. Efficacy of Silicate-Substituted Calcium Phosphate Ceramic in Posterolateral Instrumented Lumbar Fusion. *Spine* **2010**, *35*, E1058–E1063. [[CrossRef](#)]
79. Bianco, A.; Cacciotti, I.; Lombardi, M.; Montanaro, L. Si-substituted hydroxyapatite nanopowders: Synthesis, thermal stability and sinterability. *Mater. Res. Bull.* **2009**, *44*, 345–354. [[CrossRef](#)]
80. Dong, G.; Zheng, Y.; He, L.; Wu, G.; Deng, C. The effect of silicon doping on the transformation of amorphous calcium phosphate to silicon-substituted α -tricalcium phosphate by heat treatment. *Ceram. Int.* **2016**, *42*, 883–890. [[CrossRef](#)]
81. Bigi, A.; Cojazzi, G.; Panzavolta, S.; Ripamonti, A.; Roveri, N.; Romanello, M.; Suarez, K.N.; Moro, L. Chemical and structural characterization of the mineral phase from cortical and trabecular bone. *J. Inorg. Biochem.* **1997**, *68*, 45–51. [[CrossRef](#)]
82. Driessens, F.C.M. The mineral in bone, dentin and tooth enamel. *Bull. Des. Soc. Chim. Belges.* **2010**, *89*, 663–689. [[CrossRef](#)]
83. Sroka-Bartnicka, A.; Borkowski, L.; Ginalska, G.; Ślósarczyk, A.; Kazarian, S.G. Structural transformation of synthetic hydroxyapatite under simulated in vivo conditions studied with ATR-FTIR spectroscopic imaging. *Spectrochim. Acta Part A Mol. Biomol. Spectrosc.* **2017**, *171*, 155–161. [[CrossRef](#)]
84. Doi, Y. Sintered carbonate apatites as bone substitutes. *Cells Mater.* **1997**, *7*, 111–122.
85. Montel, G.; Bonel, G.; Heughebaert, J.C.; Trombe, J.C.; Rey, C. New concepts in the composition, crystallization and growth of the mineral component of calcified tissues. *J. Cryst. Growth* **1981**, *53*, 74–99.
86. Jarcho, M.; Kay, J.F.; Gumaer, K.I.; Doremus, R.H.; Drobeck, H.P. Tissue, cellular and subcellular events at a bone-ceramic hydroxylapatite interface. *J. Bioeng.* **1977**, *1*, 79–92. [[PubMed](#)]
87. LeGeros, R.Z. Properties of Osteoconductive Biomaterials: Calcium Phosphates. *Clin. Orthop. Relat. Res.* **2002**, *395*, 81–98. [[CrossRef](#)] [[PubMed](#)]

88. Hayek, E.; Böhler, W.; Lechleitner, J.; Petter, H. Hydrothermalsynthese von Calcium-Apatiten. *Zeitschrift für Anorg. Und Allg. Chem.* **1958**, *295*, 241–246. [[CrossRef](#)]
89. Young, R.A.; Bartlett, M.L.; Spooner, S.; Mackie, P.E.; Bonel, G. Reversible high temperature exchange of carbonate and hydroxyl ions in tooth enamel and synthetic hydroxyapatite. *J. Biol. Phys.* **1981**, *9*, 1–26. [[CrossRef](#)]
90. Young, R.A. Biological Apatite vs Hydroxyapatite at the Atomic Level. *Clin. Orthop. Relat. Res.* **1975**, *113*, 249–262. [[CrossRef](#)]
91. LeGeros, R.Z.; Trautz, O.R.; Klein, E.; LeGeros, J.P. Two types of carbonate substitution in the apatite structure. *Experientia* **1969**, *25*, 5–7. [[CrossRef](#)]
92. Landi, E.; Celotti, G.; Logroscino, G.; Tampieri, A. Carbonated hydroxyapatite as bone substitute. *J. Eur. Ceram. Soc.* **2003**, *23*, 2931–2937. [[CrossRef](#)]
93. Merry, J.C.; Gibson, I.R.; Best, S.M.; Bonfield, W. Synthesis and characterization of carbonate hydroxyapatite. *J. Mater. Sci. Mater. Med.* **1998**, *9*, 779–783. [[CrossRef](#)]
94. Ingram, G.S. The Role of Carbonate in Dental Mineral. *Caries Res.* **1973**, *7*, 217–230. [[CrossRef](#)] [[PubMed](#)]
95. Hallsworth, A.S.; Weatherell, J.A.; Robinson, C. Loss of Carbonate during the First Stages of Enamel Caries. *Caries Res.* **1973**, *7*, 345–348. [[CrossRef](#)] [[PubMed](#)]
96. Askar, H.; Krois, J.; Göstemeyer, G.; Bottenberg, P.; Zero, D.; Banerjee, A.; Schwendicke, F. Secondary caries: What is it, and how it can be controlled, detected, and managed? *Clin. Oral Investig.* **2020**, *24*, 1869–1876. [[CrossRef](#)] [[PubMed](#)]
97. Magalhães, A.C.; Wiegand, A.; Rios, D.; Honório, H.M.; Buzalaf, M.A.R. Insights into preventive measures for dental erosion. *J. Appl. Oral Sci.* **2009**, *17*, 75–86. [[CrossRef](#)]
98. Frauenfelder, H.; Fenimore, P.; McMahon, B. Hydration, slaving and protein function. *Biophys. Chem.* **2002**, *98*, 35–48. [[CrossRef](#)]
99. Bagchi, B. Water dynamics in the hydration layer around proteins and micelles. *Chem. Rev.* **2005**, *105*, 3197–3219. [[CrossRef](#)]
100. Yang, A.H.C.; Hou, J.; Chen, V.; Xu, Z.K. Surface and interface engineering for organic–inorganic composite membranes. *J. Mater. Chem. A* **2016**, *4*, 9716–9729. [[CrossRef](#)]
101. Tanaka, M.; Sato, K. Thermal Characterization of Novel Polymers for Biomedical Applications. *Netsusokutei = Calorim. Therm. Anal.* **2012**, *39*, 151–157.
102. Tanaka, M.; Sato, K.; Kitakami, E.; Kobayashi, S.; Hoshihara, T.; Fukushima, K. Design of biocompatible and biodegradable polymers based on intermediate water concept. *Polym. J.* **2015**, *47*, 114–121. [[CrossRef](#)]
103. Gómez-Morales, J.; Iafisco, M.; Delgado-López, J.M.; Sarda, S.; Drouet, C. Progress on the preparation of nanocrystalline apatites and surface characterization: Overview of fundamental and applied aspects. *Prog. Cryst. Growth Charact. Mater.* **2013**, *59*, 1–46.
104. Rossi, A.M.; Prado da Silva, M.H.; Ramirez, A.J.; Biggemann, D.; Caraballo, M.M.; Mascarenhas, Y.P.; Eon, J.G.; Moure, G.T. Structural Properties of Hydroxyapatite with Particle Size Less Than 10 Nanometers. *Key Eng. Mater.* **2007**, *330*, 255–258. [[CrossRef](#)]
105. Delgado-López, J.M.; Iafisco, M.; Rodríguez, I.; Tampieri, A.; Prat, M.; Gómez-Morales, J. Crystallization of bioinspired citrate-functionalized nanoapatite with tailored carbonate content. *J. Acta Biomater.* **2012**, *8*, 3491–3499. [[CrossRef](#)] [[PubMed](#)]
106. Bolis, V.; Busco, C.; Martra, G.; Bertinetti, L.; Sakhno, Y.; Ugliengo, P.; Chiatti, F.; Corno, M.; Roveri, N. Coordination chemistry of Ca sites at the surface of nanosized hydroxyapatite: Interaction with H₂O and CO. *Phil. Trans. R. Soc. A* **2012**, *370*, 1313–1336. [[CrossRef](#)] [[PubMed](#)]
107. Tagaya, M. In situ QCM-D study of nano-bio interfaces with enhanced biocompatibility. *Polym. J.* **2015**, *47*, 599–608. [[CrossRef](#)]
108. Kasemo, B. Biological surface science. *Surf. Sci.* **2002**, *500*, 656–677. [[CrossRef](#)]
109. El-Ghannam, A.; Ducheyne, P.; Shapiro, I.M. Effect of serum proteins on osteoblast adhesion to surface-modified bioactive glass and hydroxyapatite. *J. Orthop. Res.* **1999**, *17*, 340–345. [[CrossRef](#)] [[PubMed](#)]
110. Rouahi, M.; Champion, E.; Gallet, O.; Jada, A.; Anselme, K. Physico-chemical characteristics and protein adsorption potential of hydroxyapatite particles: Influence on in vitro biocompatibility of ceramics after sintering. *Colloids Surf. B Biointerfaces* **2006**, *47*, 10–19. [[CrossRef](#)] [[PubMed](#)]
111. Panda, R.N.; Hsieh, M.F.; Chung, R.J.; Chin, T.S. FTIR, XRD, SEM and Solid State NMR Investigations of Carbonate-containing Hydroxyapatite Nano-particles Synthesized by Hydroxide-gel Technique. *J. Phys. Chem. Solids* **2003**, *64*, 193–199. [[CrossRef](#)]
112. Rey, C.; Combes, C.; Drouet, C.; Sfihi, H.; Barroug, A. Physico-chemical properties of nanocrystalline apatites: Implications for biominerals and biomaterials. *Mater. Sci. Eng.* **2007**, *27*, 198–205. [[CrossRef](#)]
113. Bertinetti, L.; Drouet, C.; Combes, C.; Rey, C.; Tampieri, A.; Coluccia, S.; Martra, G. Surface Characteristics of Nanocrystalline Apatites: Effect of Mg Surface Enrichment on Morphology, Surface Hydration Species, and Cationic Environments. *Langmuir* **2009**, *25*, 5647–5654. [[CrossRef](#)]
114. Cazalbou, S.; Eichert, D.; Ranz, X.; Drouet, C.; Combes, C.; Harmand, M.F.; Rey, C. Ion exchanges in apatites for biomedical application. *J. Mater. Sci. Mater. Med.* **2005**, *16*, 405–409. [[CrossRef](#)] [[PubMed](#)]
115. Drouet, C.; Carayon, M.T.; Combes, C.; Rey, C. Exchange of biologically relevant ions on nanocrystalline apatites. *Geochim. Cosmochim. Acta* **2005**, *69*, A69.
116. Autefage, H.; Briand-Mésange, F.; Cazalbou, S.; Drouet, C.; Fourmy, D.; Gonçalves, S.; Salles, J.P.; Combes, C.; Swider, P.; Rey, C. Adsorption and release of BMP-2 on nanocrystalline apatite-coated and uncoated hydroxyapatite/beta-tricalcium phosphate porous ceramics. *J. Biomed. Mater. Res. Part B* **2009**, *91*, 706–715. [[CrossRef](#)] [[PubMed](#)]
117. Bruijn, J.D.; Bovell, Y.P.; van Blitterswijk, C.A. Structural arrangements at the interface between plasma sprayed calcium phosphates and bone. *Biomaterials* **1994**, *15*, 543–550. [[CrossRef](#)]

118. Daculsi, G.; LeGeros, R.Z.; Nery, E.; Lynch, K.; Kerebel, B. Transformation of biphasic calcium phosphate ceramics in vivo: Ultrastructural and physicochemical characterization. *J. Biomed. Mater. Res.* **1989**, *23*, 883–894. [[CrossRef](#)]
119. Schepers, E.; Clercq, M.D.; Ducheyne, P.; Kempeneers, R. Bioactive glass particulate material as a filler for bone lesions. *J. Oral Rehabil.* **1991**, *18*, 439–452. [[CrossRef](#)]
120. Porter, A.E.; Patel, N.; Skepper, J.N.; Best, S.M.; Bonfield, W. Comparison of in vivo dissolution processes in hydroxyapatite and silicon-substituted hydroxyapatite bioceramics. *Biomaterials* **2003**, *24*, 4609–4620. [[CrossRef](#)]
121. Qiu, Z.; Noh, I.; Zhang, S. Silicate-doped hydroxyapatite and its promotive effect on bone mineralization. *Front. Mater. Sci.* **2013**, *7*, 40–50.
122. Tang, P.F.; Li, G.; Wang, J.F.; Zheng, Q.J.; Wang, Y. Development, Characterization, and Validation of Porous Carbonated Hydroxyapatite Bone Cement. *J. Biomed. Mater. Res. B Appl. Biomater.* **2009**, *90*, 886–893. [[CrossRef](#)]

Disclaimer/Publisher's Note: The statements, opinions and data contained in all publications are solely those of the individual author(s) and contributor(s) and not of MDPI and/or the editor(s). MDPI and/or the editor(s) disclaim responsibility for any injury to people or property resulting from any ideas, methods, instructions or products referred to in the content.